University of Siegen
Department of Physics
Experimental Particle Physics

Deutsches Elektronen Synchrotron (DESY)
Photo injector test facility in Zeuthen (PITZ)

Resolution of different beam size read-out systems at PITZ

A master thesis by: Mohammad Rahmatullah Tanha
Supervised by: Prof. Dr. Claus Grupen and Dr. Frank Stephan

Zeuthen 2010

Abstract

The **P**hoto **I**njector **T**est facility in **Z**euthen (PITZ) is one of the research groups of the DESY branch at Zeuthen - Brandenburg. The major goal of this facility is to develop and optimize a high brightness electron beam sources as demanded for the **F**ree electron **LAS**er in **H**amburg (FLASH) and the European XFEL.

PITZ investigates the characteristics of the emitted electron beam in great detail. The Characterization includes studies on the transverse and longitudinal phase-space distribution of the electron beam. Main sources of information on the phase-space distribution are the measured electron beam distributions on observation screens. These distributions are obtained from scintillating or OTR screens with a CCD camera and appropriate read-out optics. Each element of these read-out systems contributes to the resolution of the measurement. The read-out system is based on two main technical components: **O**ptical **T**ransition **R**adiation (OTR) and **Y**ttrium **A**luminium **G**arnet (YAG) screens. [1]

This thesis describes the resolution limitations emerging in the beam size measurements. Photon yield from different screens, factors which contribute to screen's saturation limits for various beam momenta, rms spot size measurements and the resolution of the optical system using different lenses are discussed.

Table of contents

1. Introduction

A device which uses electric fields for propelling charged particles to higher energies is called Particle Accelerator. Different types of such devices have been designed and built. Two general types of these machines Circular Accelerator and **Lin**ear **Ac**celerator (LINAC) are commonly used as particle accelerator. Over 70 different types of particle accelerators have been operated world wide so far [2].

The PITZ facility contains a small LINAC. It was built to develop and optimize a high brightness electron beam sources as demanded for European X-ray Free Electron Laser (XFEL) project.[3] The required beam quality for XFEL is: 0.9 mm mrad normalized projected emittance at the injector for 1nC bunch charge. [4]

The charged particle bunch profiles can be measured using many different diagnostic tools: The most popular one of PITZ are OTR and YAG screens.

This thesis discusses two main parts: The contribution to screens and the optical read-out system to the overall resolution of the system. The work is divided into five major sections. The first section gives an introduction to the whole procedure of this work. The second section introduces the basics; and theoretical aspects of the YAG and OTR screens and the optics design. The third section describes the PITZ facility setup. In the fourth section the theoretical and experimental aspects of those factors which contribute to the resolution of the read-out system are

discussed. Simulation and measurement results for the optical system components are presented and compared. The fifth and final section contains the conclusions of the thesis.

2. Background and theoretical aspects

2.1. Theoretical aspects

As mentioned above, PITZ aims to develop a high brightness electron beam source which meets the requirements of the European XFEL project. The area occupied by the moving particles of the beam in 6D phase space (x,y,z,p_x,p_y,p_z) is called beam emittance. Two different types of emittances are introduced: the longitudinal emittance that represents the (z, p_z) projection of the 6D phase space and is parallel to the incident beam velocity direction, and the transverse emittance which is perpendicular to the incident beam direction and is represented by the (x,y,p_x,p_y) projection of the 6D phase space.

The normalized beam transverse emittance obtained in the experiment is calculated in the following expression: [5]

$$\varepsilon_N = \gamma\beta\sqrt{X_{rms}^{\ 2} X'^{\ 2}_{rms} - \langle XX' \rangle^2} \qquad (1)$$

Where $\gamma = \frac{E_0}{E}$ and $\beta = \frac{V}{c}$ are the Lorentz factor for energy and velocity of the particle respectively, α presents the beam RMS size, β represents the beam rms divergence and γ is the XX' correlations term.

E = Particle energy

E_0 = Particle energy at rest

V = Particle velocity

C = Velocity of light

$$\alpha = X_{rms} = \sqrt{\left\langle \left(X - \langle X \rangle\right)^2 \right\rangle}$$

$$\beta = X'_{rms'} = \sqrt{\left\langle \left(X' - \langle X' \rangle\right)^2 \right\rangle}$$

$$\gamma = \langle XX' \rangle^2 = \left\langle \left(X - \langle X \rangle\right)\left(X' - \langle X' \rangle\right) \right\rangle$$

An example for the beam emittance is shown in Fig1. As the sensitivity is limited due to measuring devices and conditions, therefore no absolute emittance can exist in experiments, so we usually measure rms (root-mean-square) quantities from the beam size observed on the screens. The rms beam emittance is derived from such rms quantities. E.g. for a horizontal transverse emittance calculation one needs to measure the horizontal transverse rms beam size and the horizontal rms beam divergence.

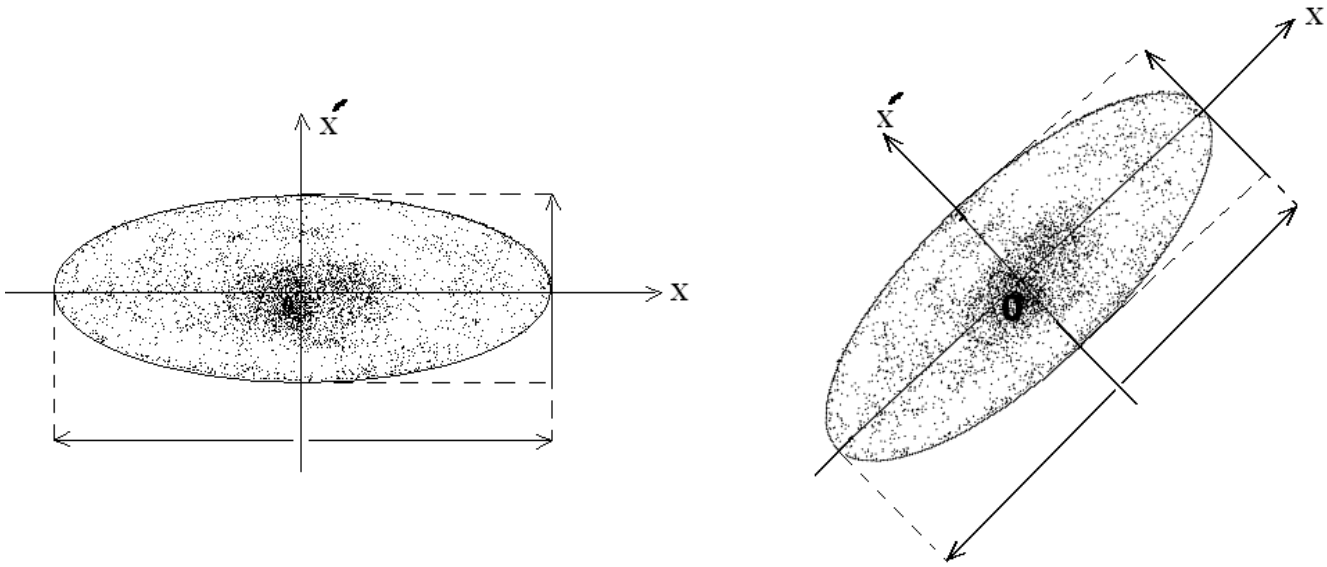

Fig1: The schematic of beam emittance and the corresponding beam ellipse

PITZ uses two main diagnostic techniques for beam size measurements: YAG and OTR screens and Wire Scanners, where this work concentrates only on YAG/OTR systems.

2.2 MTF (**M**odulation **T**ransfer **F**unction)

The sharpness of an imaging system can be characterized by the MTF (**M**odulation **T**ransfer **F**unction). The MTF is the contrast at a given spatial frequency. The spatial frequency is typically measured in cycles or line pairs per millimetre (Lp/mm) Lp/mm is most appropriate for film and cameras, where formats are relatively fixed, but cycles/pixel (c/p) or line widths per picture height

(LW/PH) may be more appropriate for digital cameras, which have a wide variety of sensor sizes. High spatial frequencies give finer details about the image. The more extended response of the optical system leads to finer details of the image which can be obtained sharper. Contrast levels from 2% to 100% are illustrated in Fig2 for a varying frequency of the sinusoidal pattern. [6]

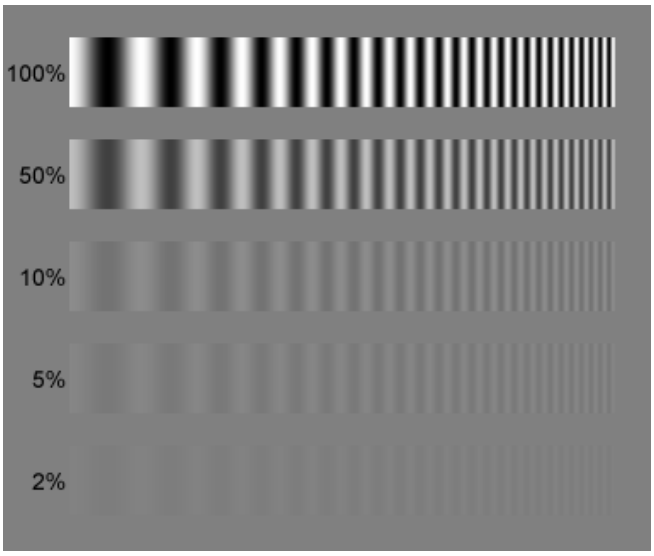

Fig2: The contrast level from 2% - 100% for a Sinusoidal pattern with varying frequency is shown

As shown in Fig2 by moving from lower to higher contrasts the number of lines per mm is easier to detect and the finer lines in the image are becoming more clear and visible.

The MTF is normalized to 100%. The standard and known value of measuring the MTF for determining the resolution of an optical system is at 10% - 15% of MTF cut off, which means that at this percentage of reduced contrast it is determined how many lines or cycles per millimeter can be resolved by the system (system resolution at 10% or 15% of MTF)? In this thesis MTF 15% cut-off in modulation is used for both measurements and simulations. A typical MTF plot is shown in Fig3. The MTF can be defined as: [6]

$$MTF(f) = 100\% * C(f) / C(0) \qquad (2)$$

Black-White Contrast C (0) = $(V_W - V_B)/ (V_W + V_B)$

V_B = the minimum luminance for black areas at low spatial frequencies

V_W = the maximum luminance for white areas at low spatial frequencies

Contrast at spatial frequency C (f) = $(V_{max} - V_{min})/(V_{max} + V_{min})$

V_{min} = Minimum luminance for a pattern near spatial frequency f ("negative peak")

V_{max} = Maximum luminance for a pattern near spatial frequency f ("peak")

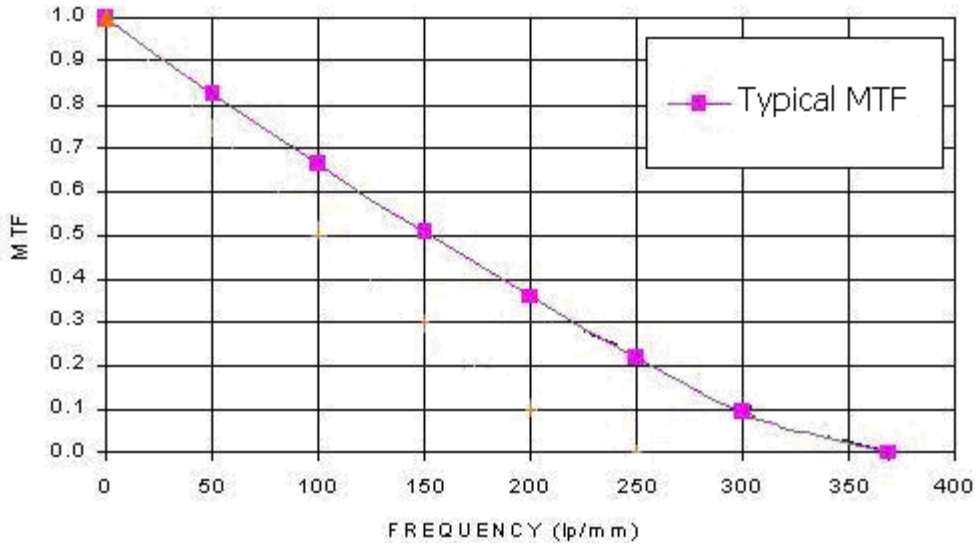

Fig3: A typical MTF plot for an optical system performance

2.3 Depths of focus and depth of field

Interesting factors which can affect the resolution are the misalignment of cameras or screens. These factors are called depth of focus and depth of field, respectively. Alignment accuracy is defined by the depth of focus and depth of field.

By definition depth of focus is the extent of the region around the image plane in which the image will appear with the same sharpness. Depth of field shows the extent of the region around the optical axis in which the image will appear to be sharp (in focus). Both depth of focus and field are strongly dependent on the lens aperture and working distance. Displacement of camera and screen causes image

blurring. If θ is the blurring angle which measures the blurring rate in terms of angle then one can write: [7]

$$\theta = p * D \qquad (3)$$

Where p is the aperture size of the lens and D is called “Delta Dioptres” which shows the change in curvature of the lens originated from change in object location and image location for depth of field and depth of focus, respectively. It shows that to some extent the larger the aperture the more the image is blurred. The aperture size is focal length and f-number dependent.

2.4 Diffraction and aberration limits

The resolution of an optical system is a combination of the resolution of the camera as well as the lenses. For a better sharpness one needs to have alignment within the depth of field. Light travels in straight lines through uniform air, however it begins to "diffract" while crossing a small hole e.g. (the lens aperture) the effect becomes significant for small apertures. The diffraction law states that a sharp point in an object will not correspond to a sharp point in the image.

The best focused spot of light limited by light diffraction from a perfect lens is called "Airy disc". This disc has a certain diameter, which varies with the aperture of the imaging system. The smaller the aperture the larger the disc and the

larger the disc, the lower the resolution is. One concludes that the resolving power of the lens is aperture size dependent. When the diameter of the airy disk's central peak becomes large relative to the pixel size in the camera it begins to have a visual impact on the image. Alternatively, if two airy disks come any closer than half their width they are also no longer resolvable (Raleigh criterion). So at the end it turns out that there is a limit in between which is the border between overlapping of two airy disks caused by very close aperture which causes two diverging photon lines which are irresolvable. These limits and their condition are shown schematically in Fig4a, b. Since Parallel light rays which pass through a small aperture begin to diverge and interfere with one another. This becomes more significant as the size of the aperture decreases relative to the wavelength of light passing through, but occurs to some extent for any size of aperture or concentrated light source. Since the divergent rays now travel different distances, some move out of phase and begin to interfere with each other, adding in some places and partially or completely cancelling out in others. This interference produces a diffraction pattern with peak light intensities where the amplitude of the light waves add and less light where they cancel out Fig4b.

The diffraction limit depends on the incident wave length and the f-number or the focal length of the lenses. The circular aperture is called diameter of the central airy is:

$$D = 2.43932 \times \lambda \times \text{f-number}$$

Where D is the diameter of the Airy disk in mm, λ represents the wave length and f-number F=f/4. From here one can obtain: d = 1, 22 λF where d is the rms spotsize of the Gaussian shape Airy disk. [8]

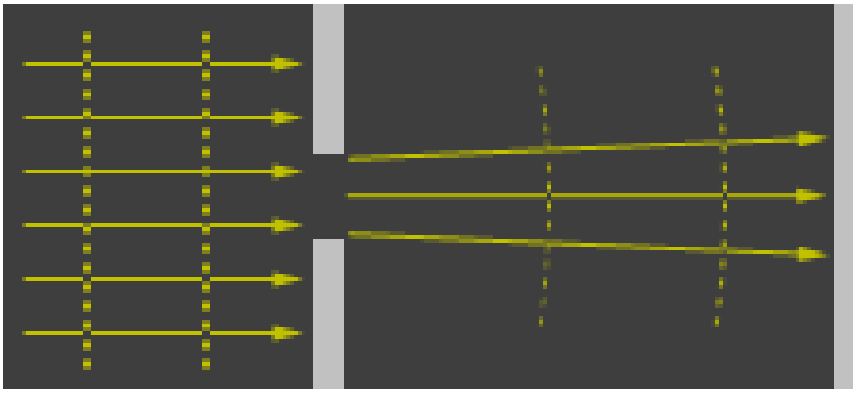

Fig4a: Larger aperture opening

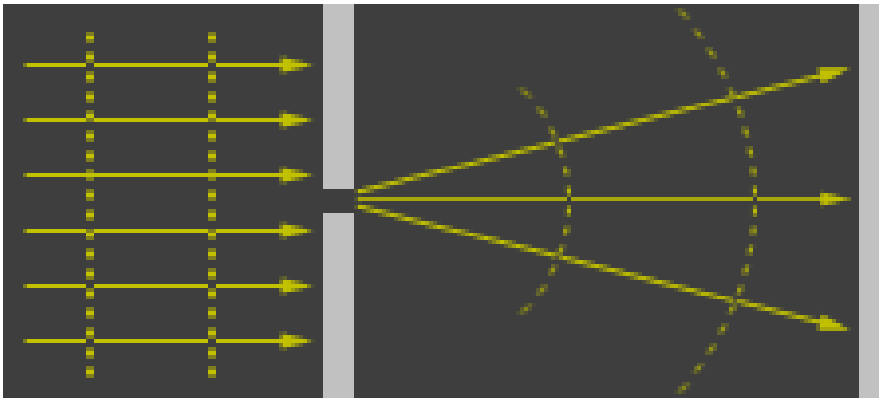

Fig4b: Smaller aperture opening

Fig4a, b diffraction and aberration limits effects

2.5 Optical Aberrations

In an ideal optical system, all rays of light from a point in the object plane would converge to the same point in the image plane, forming a clear image. The influences which cause different rays to converge to different points are called aberrations. [9] Several types of aberrations are identified in imaging processes, one of them for polychromatic light is chromatic aberration or (CA), this is a kind of distortion in the image which originates from lens disability in focusing the different colors to a single convergence point; this also leads to the image blurring. This disability of the lens refers to the different refractive index of the lens to the different colors or wave lengths, high refractive index for short wave lengths and vice versa. These aberrations appear as fringes of colors in the boundaries of two different dark – bright parts of the image.

Chromatic aberration can be reduced and corrected noticeably by using an achromat lens (Achromatic Doublet) which is made of a compound of materials with different dispersions. This achromat will make possible to focus different wavelengths to one single point. The chromatic aberration effect is shown in Fig5. [10].

The best correction occurs when the following condition is fulfilled:

$$f_1 * V_1 + f_2 * V_2 = 0 \qquad (4)$$

Where V_1 , V_2 are the Abbé numbers of the materials and f_1,f_2 are the focal lengths of two glued lenses , $V = \frac{n_D - 1}{n_F - n_C}$ where n_D , n_F and n_C are the materials wave lengths at the wave lengths of 589.2 nm , 486.1 nm and 656.3 nm respectively.[10].

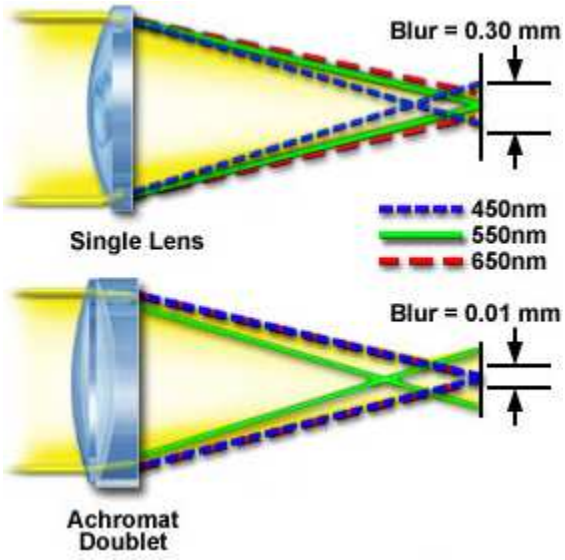

Fig5: The effect of an achromat in decreasing the chromatic aberrations. [11]

3. PITZ Facility setup and some components

3.1 PITZ Facility setup

As mentioned earlier PITZ (**P**hoto **I**njector **T**est facility at DESY in **Z**euthen) was established to develop electron sources demanded for example for the European XFEL project.

The photo injector contains an RF gun cavity with a Cs_2Te photo cathode. A laser pulse at ultraviolet wavelength is used to produce the electron beam of 20 ps pulse duration. The electron bunch is accelerated by the radio frequency electromagnetic field and within a few millimeters the electron on the beam reach almost the speed of light. Based on Coulomb's law the electrons repel each other. The electron bunch is focused by a strong magnetic field produced by a solenoid placed around the electron source. The gun section is followed by low energy diagnostics, such as a spectrometer and several scintillating screens. The electrons trajectory is controlled further by steering magnets. The downstream accelerating cavity (Booster Cavity) increases the beam energy up to about 25 MeV/c; the diagnostics after the booster is referred to as high energy diagnostics. For the emittance measurement slits with 10μm and 50μm opening are placed in the beam axis, these slits are movable horizontally and vertically by two actuators. This part

is called EMSY (**E**mittance **M**easurement **Sy**stem) station and is composed of slit masks or hole masks and screen stations at the EMSY position as well as another screen stations further downstream. All screen stations are observed by CCD cameras. As mentioned in the introductory chapter, the electron beam observation at the screen station is performed by using YAG/OTR screens with 45˚/90˚ geometry accompanied by optical components such as achromates and a CCD camera. The whole optical system is called TV station. 17 TV stations are installed along the beam pipe for imaging and measuring the electron beam profile. The cause for having different TV stations is controlling the scan along the whole beamline and specific measurement techniques at each station. In order to have high enough signal over noise ratio after the electron beam scattering from the slit one needs to use the closer TV station after the slit for low electron beam charges. The schematic layout of the current PITZ set up is shown in the Fig6.

From left to right one sees the RF (Radio frequency) Gun with the solenoids, steering coils, screen stations with and without Faraday cups, the low energy dispersive arm (LEDA) equipped with streak camera read-out, beam position monitors, the booster cavity, different screen stations equipped with OTR/YAG screens, high energy dispersive arm HEDA (in a real PITZ 1.8 setup wire scanner, tomography section and HEDA2 is added as well) and finally a beam dump. [12]

Current typical PITZ beam parameters are:

Max Mean Momentum: ~ 20MeV/c

Charge: ~ 1 nC

Min Emittance: 0.9 mm*mrad at 1 nC

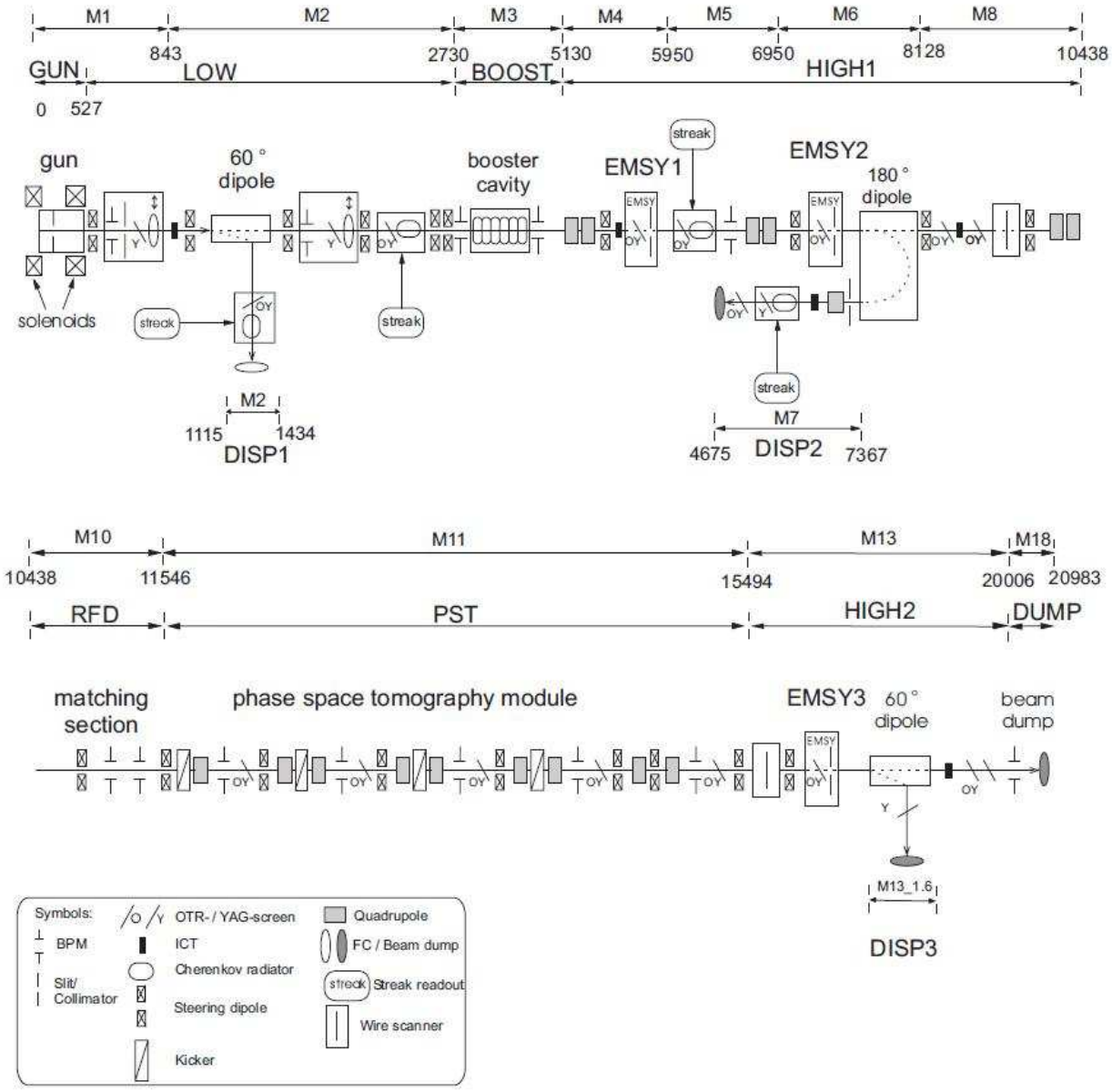

Fig6: Schematic layout of the current PITZ setup

3.2. OTR Screen

OTR (Optical Transition Radiation) is produced when a charged particle crosses a boundary of two different media with different optical densities. [13]. Moving charges are producing electromagnetic fields with the dielectric constant ε; these fields are always media dependent. The change to these electromagnetic fields is recognized at the boundary of two media by the emission of radiation. This radiation is called Optical Transition Radiation.

OTR radiation is produced in a wide spectrum from RF to X – ray, depending on the energy in the source, the maximum lies on optical wavelength or visible light range. An OTR screen is a piece of aluminium foil on a silicon wafer which is mounted at 45° with respect to the incident electron beam. OTR screen is thin compared to a YAG screen, but it still disturbs the beam quality. As shown in Fig7 electrons hit the screen, a forward and a backward radiation is produced. The produced visible light is then focused by an optical system to a CCD camera.

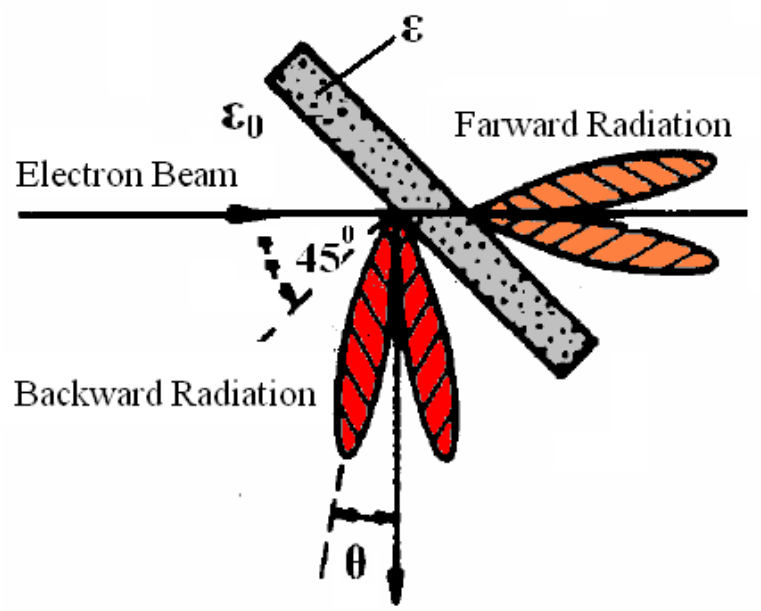

Fig7: OTR photons propagate in the forward and in the backward directions

The intensity of the radiation is beam energy dependent ($E = \gamma mc^2$) and according to Maxwell's equations considering a vacuum-metal boundary condition the radiation intensity angular distribution is described by [14]:

$$I_\theta = \frac{d^2 I}{d\omega d\Omega} = \frac{q^2}{4\pi^2 c} \frac{\sin^2\theta}{(1-\beta\cos\theta)^2} = \frac{q^2}{\pi^2 c} \frac{\theta^2}{\left[\theta^2 + \gamma^{-2}\right]^2} \qquad (5)$$

Where ω is the radiation frequency, q is the electron charge, $\theta = 1/\gamma$ is the angle of emission with respect to the perpendicular direction of the electron, $\beta = 1 - 1/(2\gamma^2)$ and γ is the Lorentz factor. If the angle θ is small ($\theta << 1$) $d\Omega = 2\pi \sin\theta d\theta$ and using the expression is simplified as:

$$I_\theta = \frac{d^2 I}{d\omega d\theta} = \frac{2q^2}{\pi c} \frac{\theta^3}{(\gamma^{-2} + \theta^2)^2} \qquad (6)$$

The emitted electric field has two components: one is the plane containing the normal to the surface (Z-axis in Fig8) and the direction of observation (Vector n in Fig8) which is called the observation plane and the other one is the perpendicular to electric field. The total intensity is the sum of the intensities of both components.

The planes of incidence and observation angles are shown in Fig8:

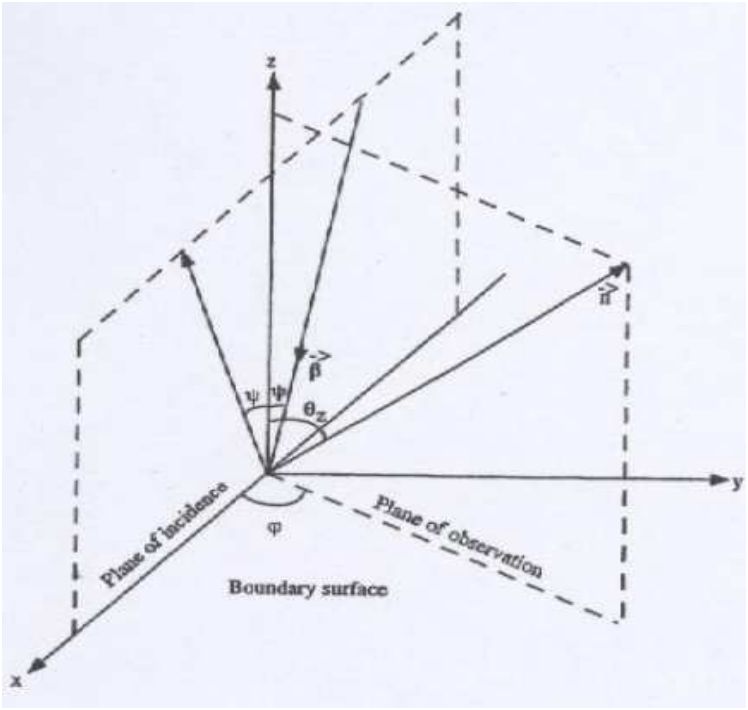

Fig8: The plane of incidence contains the velocity vector and the normal to the surface, and the plane of observation contains the observation direction and the normal to the surface [14].

According to [14] the total intensity distribution of the beam can be written as:

$$I_{\perp} = \frac{d^2 W_{\perp}}{d\omega d\Omega} = \frac{q^2}{\pi^2 c} \frac{\beta_x^2 \beta_z^4 \cos^2\theta_y \cos^2\theta_z \left|1-\varepsilon\right|^2}{\left[(1-\beta_x \cos\theta_x)^2 - \beta_z{}^2 \cos^2\theta_z\right]^2 \sin^2\theta_z}$$
$$\times \frac{1}{\left|\left(1-\beta_x \cos\theta_x + \beta_z \sqrt{\varepsilon - \sin^2\theta_z}\right)\left(\sqrt{\varepsilon - \sin^2\theta_z} + \cos\theta_z\right)\right|^2} \qquad (7)$$

Where W is the photon intensity per unit of solid angle Ω and per unit of frequency ω, $\beta_x = \beta\sin\psi$, $\beta_z = \beta\cos\psi$, $\cos\theta_x = \cos\theta_z \cos\varphi$ and $\cos\theta_y = \sin\theta_z \sin\varphi$; θ Observation angle, ε dielectric constant, φ angle between incident and observation planes and ψ is the incident angle with respect to normal line to the boundary. [14] The negative sign of the velocity vector β_z indicates that backward case has been taken into account. The sign $\perp$ means that this projection is perpendicular to the observation plane.

In a normal incidence of particle, the emitted radiation has only the parallel components. In the case of forward transition radiation the electric field is polarized in a perpendicular plane to the particle trajectory, where for backward transition radiation the field is polarized in the plane perpendicular to the direction of the reflection. The angular distribution of transition radiation is particle incident angle and the particle energy dependent.

3.3 YAG Screen

YAG: Ce (**Y**ttrium **A**luminium **G**arnet) is a cerium doped Yttrium Aluminium garnet scintillator material used for detecting the electron beam in particle accelerators. This material is chemically inert and highly radiation stable. [15]. Primary electrons, as they pass through the crystal, excite the valence electrons through Coulomb interactions, and kick them into the conductance band, producing holes. If the momentum transferred to the secondary electrons exceeds the minimum ionizing energy, they in turn produce more free particles by collisions. Eventually, all the free charge carriers thermalize around the band gap energy (7eV in YAG) and couple into excitons (electron-hole pairs). Electron-hole pair production is not a loss-free process. Energy is transferred to the holes, as well as direct dissipation into heat, through emission of optical phonons, accounts for over half of the energy deposited by the primary electrons. There are a number of models, developed to estimate the efficiency of the pair production process, and simulations suggest, that in YAG: Ce about 60,000 e-h pairs are being produced per MeV of energy transferred. An exciton travels through the crystal until the hole is trapped at the f-level of a Ce ion, Fig9. Finally the emission takes place, peaked at around 525 nm. [16]

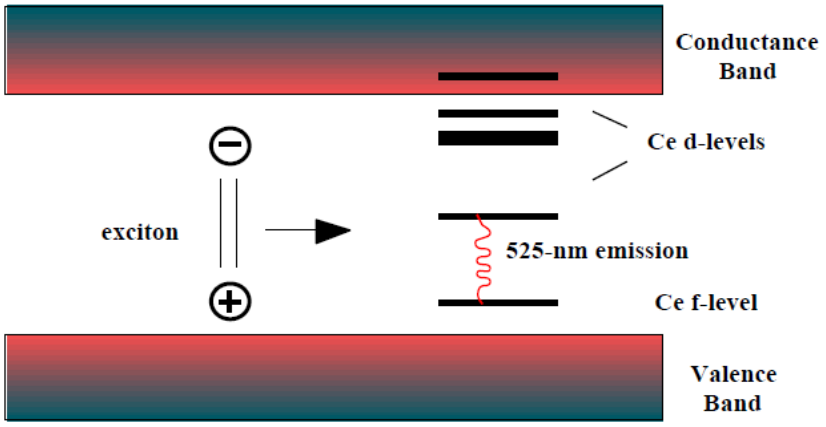

Fig9: Schematics of the scintillation process in YAG: Ce

YAG screens are available as solid crystals as well as in the powder form which is placed on a substrate material. PITZ is using the powder form of YAG. YAG can have both 45^0 and 90^0 geometry. The YAG screen geometry installed at most locations at PITZ is shown in Fig10. The advantage of 90^0 is having less depths of focus problems.

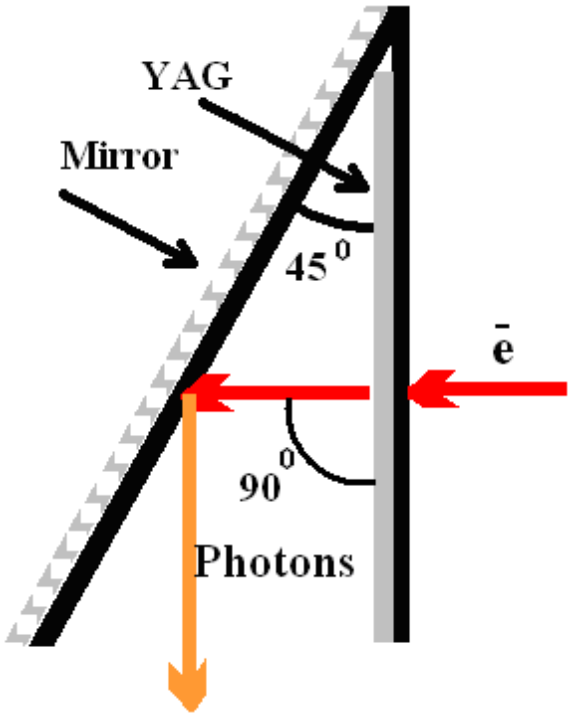

Fig10: YAG screen with 90˚ geometry toward the incident electron beam

Some of the YAG screen specifications used in PITZ is shown in table 1: [13]

Property type	Property value
Chemical formula	$Y_3\ Al_{2.5}Ga_{2.5}O_{12}$:Ce
Refraction index	1.82
Average wavelength of emitted photons	510 nm
Density of scintillator material	5.1 gr/cm^3
Thickness of silicon layer	100μm – 275μm

Table 1: Properties of YAG screen used by PITZ

3.4. Optical system design

The electron beam hits the screen, and the radiated photons pass through a quartz window out of the beam pipe. An achromat lens is used to image the screen surface on to the CCD camera. A sketch of the PITZ optics is shown in Fig11 with a 45˚ screen geometry.

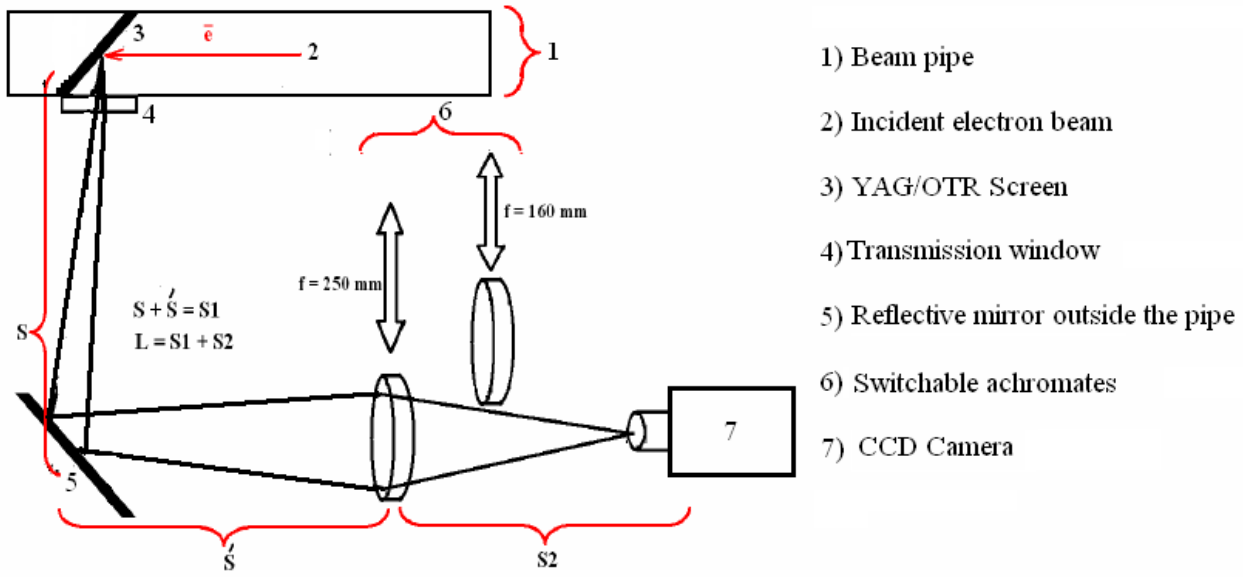

Fig11 Optical system design and components in 45˚ geometry

The mirror pointed as item number 5 in Fig11 is used to avoid possible damage of the CCD chip because of X – rays produced by the screen in the beam pipe. The two switchable achromates are used for different magnifications.

3.5. Possible uncertainties appearing during beam size measurements

Some of the uncertainties related to beam size measurements are taking place independent of the screen type but some of the uncertainties are screen type dependent. In order to understand these uncertainties one needs to know the working principles, properties and resolving power of the two different screens, OTR and YAG. The following points might contribute to the uncertainty of the measurements:

1. Screen misalignment
2. Transmission window property
3. Mirror misalignment
4. Lens magnification
5. Read-out optic alignment

1. Screen misalignment: Screen misalignment causes uncertainty. The angle between the screen and the incident electron beam is not being well enough adjusted and might differ from screen to screen. In general case, it should be 45˚/90˚ for YAG and 45˚ for OTR with respect to the electron beam direction. Changing the angle relative to the incident beam will increase or

decrease the intensity of the transmitted photons. The intensity of the beam is calculated in the following equation: [13]

$$I = \ln(1+\gamma_e{}^2\theta_m{}^2) + \frac{1}{1+\gamma_e{}^2\theta_m{}^2} \qquad (8)$$

Where I is the intensity of the photon beam, $\gamma_e = \frac{E_{Tot}}{E_0}$, E_0 is the rest mass of the electron and E_{Tot} is the total energy of the electron beam, $\theta_m = \frac{1}{\gamma_e}$ shows the optical aperture (In case of PITZ it is 0.2 rad).[19], .The uncertainty can be defined as described in the OTR response section of chapter 4.

2. Transmission window property: The absorption coefficient of the transmission window should be as small as possible. This factor is window material dependent. The absorption coefficient can be calculated from the Beer–Lambert law: [17]. PITZ uses a window made of Quartz with 3.3 mm thickness and the absorption coefficient is 0.033/mm.
3. Mirror misalignment: Inaccurate adjustment of the reflective mirror outside the pipe towards the beam or CCD also contributes to the uncertainty of the measurement. The changes in mirror's position can only occur around both transverse axes and due to the fixed focal plane and position of the CCD

camera the mirror is tightly adjusted to the girder, so that changes in longitudinal direction are impossible.

4. Lens magnification: The lens magnification is another point which contributes to the uncertainty. The emitted photon beam is a function of the electron beam size which again is related to the beam energy and intensity. These parameters contribute in choosing the preferred achromat lens for the desired magnification. Because of beam divergence, for higher momenta a smaller aperture is preferred for imaging while going to low momenta one needs a larger aperture. PITZ uses a maximum of 40 mm diameter aperture. Smaller opening of the aperture make the resolution worse because of diffraction limits of the lens. Lenses with higher magnification factors deliver higher resolution in Fig12 the aperture opening is shown: [18]

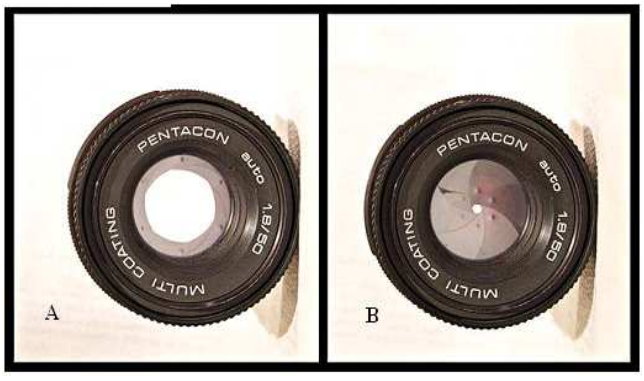

Fig12: a) half open aperture b) closed aperture

5. Read-out Optics alignment: For incorrect full optical length, the optical component such as achromates and distances between these components will contribute to limits of the measurement resolution.

4. Simulated and measured results

Reliable results require a precise processing of both experimental as well as simulated data based on the theory. As the title shows, the main goal of this thesis is to find the resolution of the read-out system which includes the influence of the screens as well as the optical system. The design of the optical system has been identified and figured out in section 3.4. The screen's response to different momenta, the optical system components and the resolution of the optical system are discussed in this chapter.

One of the screen stations in the PITZ tunnel with 160 mm and 250 mm focal length achromates was used for the measurements as well as for the simulation procedure in this thesis. The technical drawing of one of the screen stations is shown in Fig13a [19], coordinate list of some screen stations is shown in Fig13b, the screen station marked with a red ellipse (High1Scr3) were used in this work.

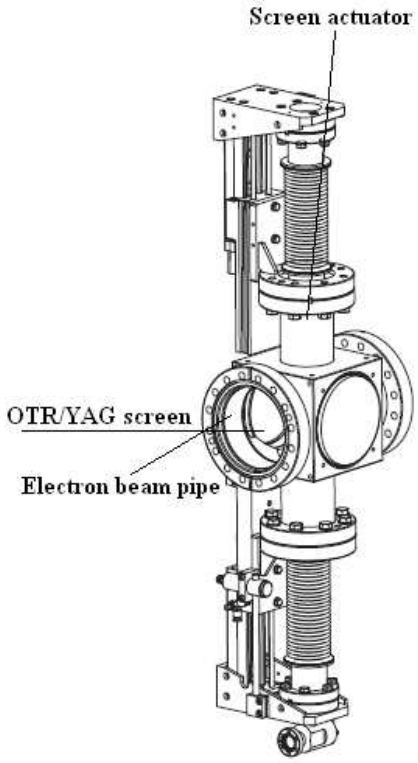

Fig13a: Simplified technical drawing of screen station [19]

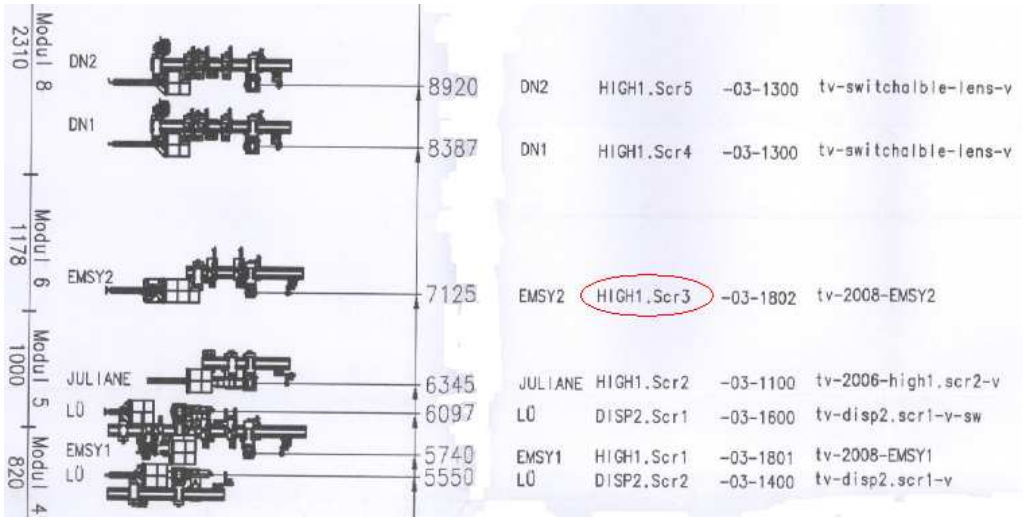

Fig13b: Coordinate list of some screen stations along the beam pipe [20]

The full properties of the optical system components for this screen station are shown in the following table 2:

Specification	First achromat	Second achromat
Focal length	250 mm	160 mm
Full length of the optical system L = S1+S2	1030 mm	1030 mm
Light path in vacuum	105.9 mm	105.9 mm
Distance between screen and achromat = S1	603 mm	832 mm
Distance between achromat and camera = S2	421 mm	190 mm
Quartz made transmission window thickness	3.3 mm	3.3 mm
Achromat thickness	11.5 mm	13.5 mm
Achromat diameter	50.8 mm	50.8 mm
Effective object diameter	10 mm	10 mm
Full aperture diameter	35 mm	35 mm
demagnification factor	- 0.70	- 0.23
CCD Camera	Prosilica 1350	Prosilica 1350
Real pixel size	9.3 μm	9.3 μm
Projected pixel size	0.013 mm	0.040 mm
Maximum incident wave length from YAG/OTR	510 nm	510 nm

Table2: List of properties of the optical system for the screen station High1Scr3

The real pixel size is a 2x2 Bind pixel value, and the projected pixel size is the ratio between the real pixel size over the magnification of each achromat. As far as the OSLO EDU software takes the absorption coefficient of the quartz transmission window into account as well, therefore when we calculate the paths of each individual parameter manually and sum them up we get a difference of around 5.5mm in comparison to the whole optical path.

4.1 OTR screen simulations

Equation (7) of section 3.2 shows the dependence of the intensity from the OTR screens relative to the incident angle ψ. This dependence is shown in Fig14.

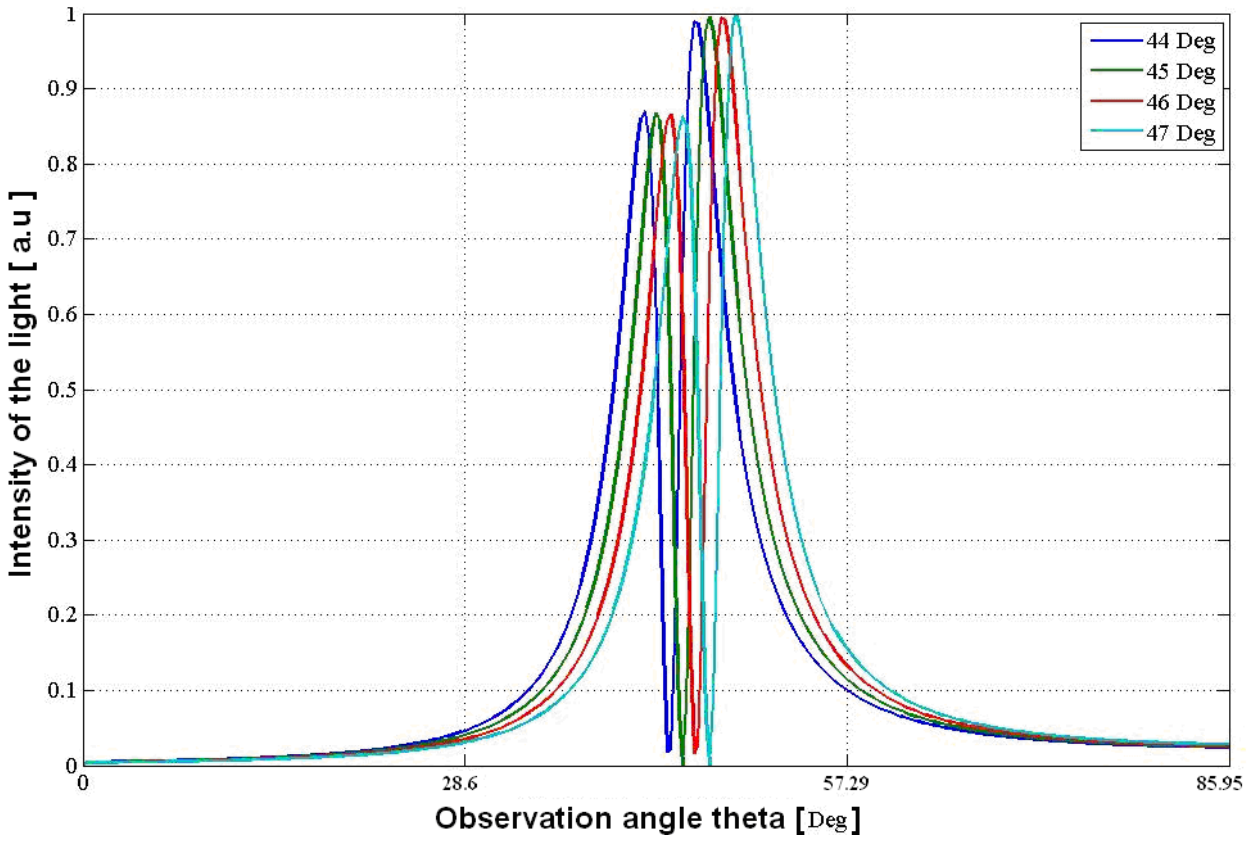

Fig14: OTR screen response for different incident angles ψ

In the above case the momentum p = 15 MeV/c is kept fixed and the incident angle ψ varies from 44º to 47º by 1º steps for θ = 2 rad. As one can see from the figure the distribution doesn't change; the only change is the shift in the position of the distribution.

The same equation (7) is used in Fig15 for investigating the OTR response to different momenta.

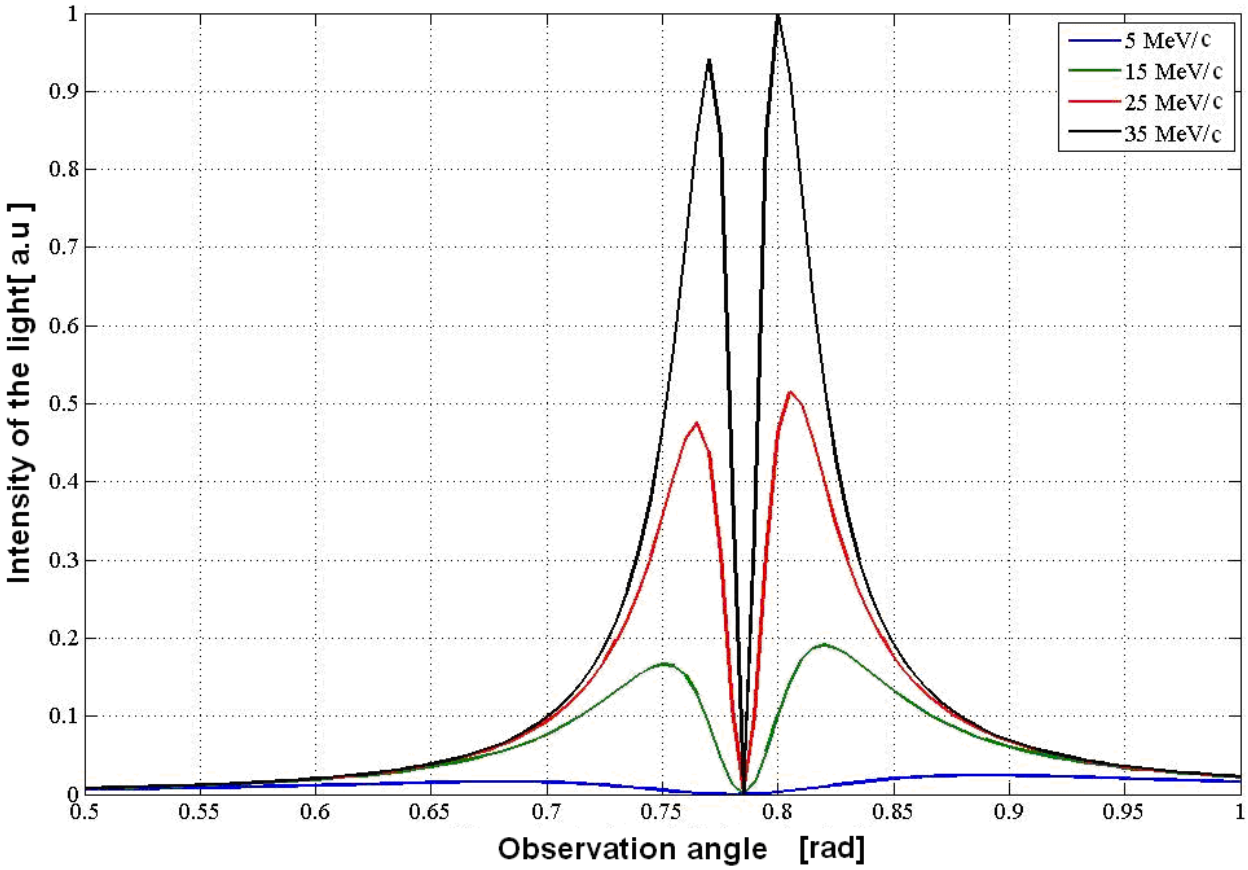

Fig15 OTR screen response for different momenta

In this case the incident angle $\psi = 45^{o}$ is kept fixed and the momentum varies from 5 MeV/c to 35 MeV/c in steps of 10 MeV/c. As one can see from the distribution in Fig15 the peak intensity increases with the momentum and as it goes to lower momenta the intensity decreases. At around 5MeV/c the distribution has low intensity and is spread over a wide angular range.

A radiator which emits stronger radiation in one direction than the other is called anisotropic. The OTR screen is an anisotropic radiator which has not the same intensity in all directions. The difference between the two shoulders of the intensity peak in Fig14 and 15 might be originated from the fact that: in the simulation, the position of the observation is not at the same angle and not at the same plane of the incident angle. OTR radiation is peaking at an angle of about $\theta=1/\gamma$ relative to the particle or centric light path (Fig7, 8 of section 3.2). When γ is small, the emission angles are not necessarily small. As γ reaches higher values, the radiation exhibits the characteristic peaked angular behavior and the asymmetry between the lobes of emitted radiation becomes weak. [13]

4.2 YAG screen simulations

The amount of light produced by YAG is proportional to the deposited energy of the incident electron beam; this is only true between threshold (the lowest energy which can cause photon production in YAG) and saturation levels.

When a charged particle crosses a medium, it is deflected by small angles so called scattering angles θ_0 which depend on the thickness and the type of material of the medium. Multiple scattering causes electron trajectory misplacement and results in beam profile image blurring. Another point to be mentioned is that there

is also a high possibility of burning the screen for higher energies of the incident particles for strongly focused beam due to the small area in which the energy is absorbed [16].The photon yield from YAG depends on the thickness of YAG layers and the momentum. The particle scattering in the screen material is originated from reactions between nuclei and electrons, so it is often called Coulomb's scattering which is shown in Fig16.

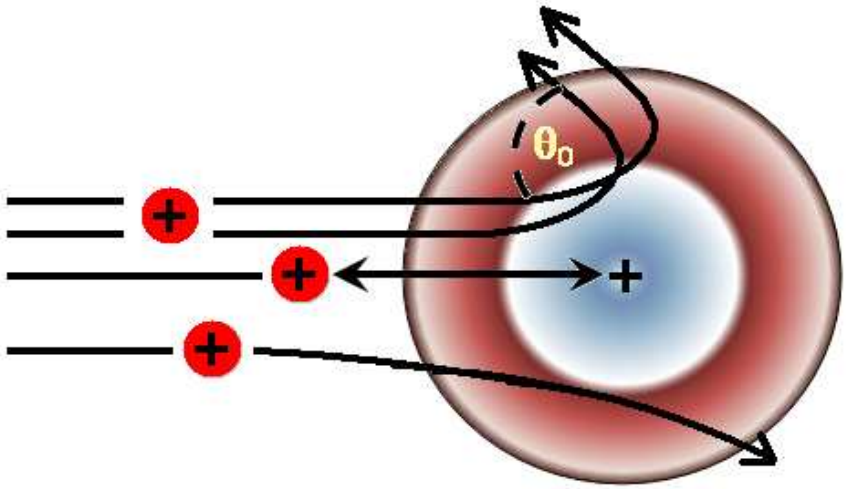

Fig16: Coulomb's scattering from a nuclei for positively charged particles

The rms scattering angle θ_0 is defined as: [21]

$$\theta_0 = \frac{13.6MeV/c}{\beta cp} z \sqrt{\frac{x}{X_0}} \left[1 + 0.038 \ln\left(\frac{x}{X_0} \right) \right] \qquad (9)$$

Where βc, p and z are velocity, momentum and charge of the incident particle respectively and x is the thickness of the medium, X_0 shows the radiation length. For PITZ case $\beta \approx 1$ and z = 1. The Coulomb's scattering distribution is nearly Gaussian for small scattering angles, but for higher scattering angles it behaves like Rutherford scattering. The scattering angle as a function of the incident electron momentum for different thicknesses of Silicon layers is shown in Fig17.

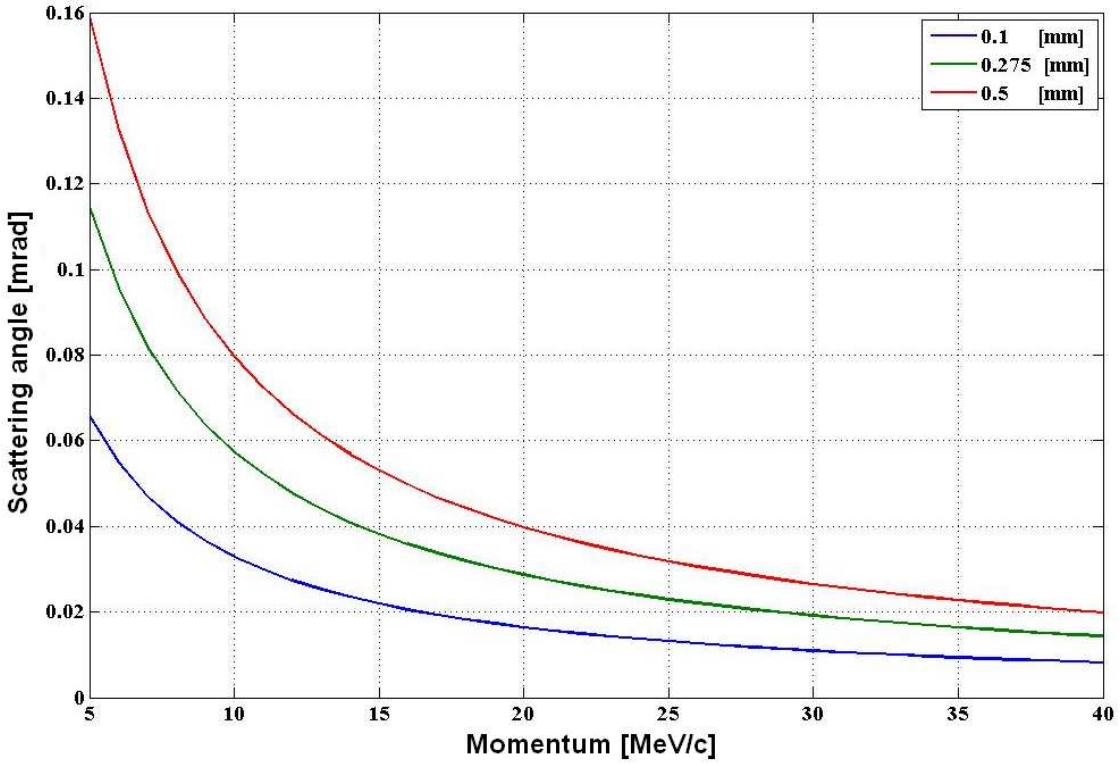

Fig17: The scattering angle as a function of the electron momentum and the YAG layer thickness

The scattering angle is getting smaller for higher momenta. The dependence of the minimum spot size on the screen for different thicknesses is shown in Fig18 and is derived in equation (10) by integrating equation (9) over the YAG layer thickness x.

$$\sigma = \int_0^x \frac{13.6MeV/c}{\beta cp} z\sqrt{\frac{x}{X_0}}\left[1+0.038\ln\left(\frac{x}{X_0}\right)\right]dx \qquad (10)$$

Where σ is the rms spot size and X_0 = 93.7 mm the radiation length assumed in the simulation.

If one considers the X value very small the integral of (10) will have an $X^{3/2}$ form which matches to the simulations plot in Fig18.The minimum spot size of the electron beam as a function of the YAG layer thickness shown in Fig18 for a momentum of 32 MeV/c.

From Fig18 one can see that the spot size of the beam on the screen is getting larger while going to higher thicknesses which results in image blurring. From here one concludes that a better resolution from YAG requires thinner YAG layers.

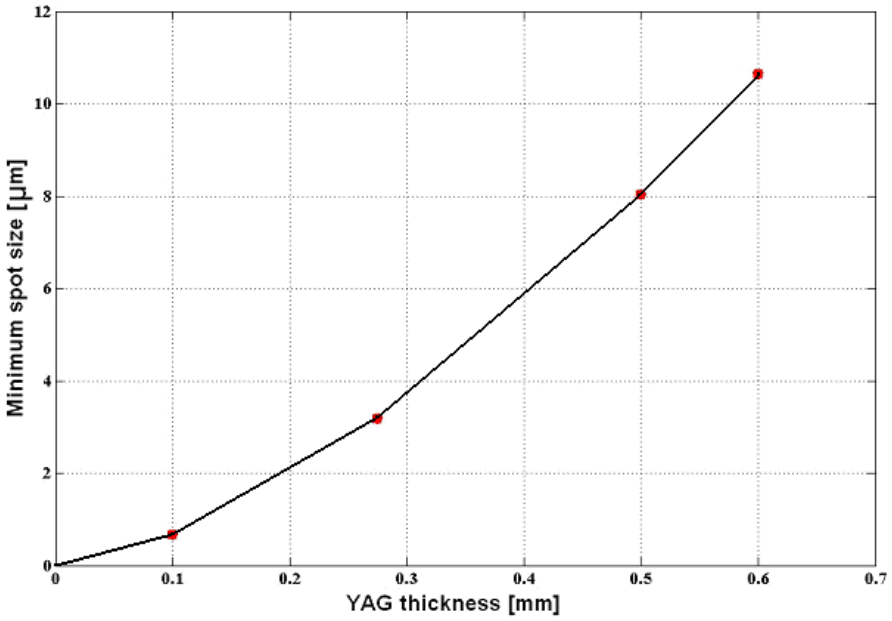

Fig18 Minimum spot size of the electron beam as a function of the YAG layer thickness

4.3 Optical system simulations and measurements

From the simulations the following results were achieved by using 20 mm aperture opening and 1030 mm full optical length of the system. The simulation and measurement results are shown in Fig19a, b, c, d for lenses having 250 mm and 160 mm focal lengths.

For simulating and measuring the MTF at 15% cut-off for the optical system, OSLO EDU software, Quick MTF software, LINOS made achromates and Prosilica 1350 CCD camera device are used. [22, 23, 24, 25] The CCD has a 9.3 mm projected Pixel size.

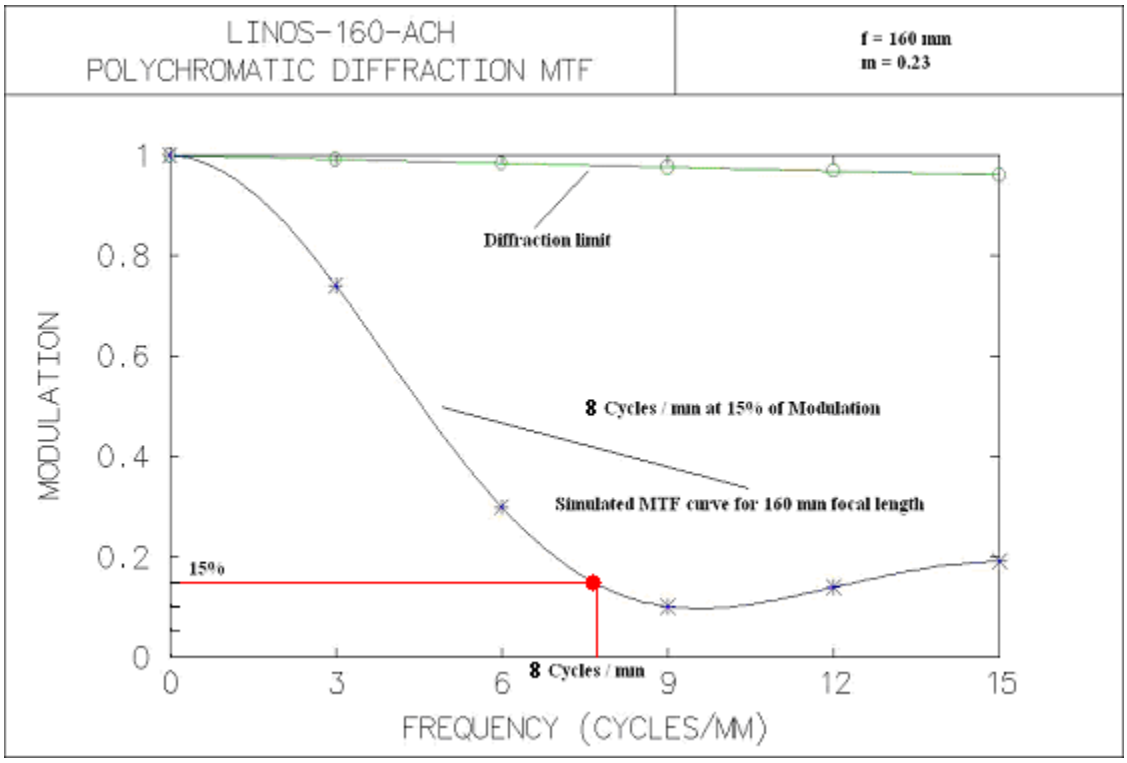

Fig19 a) Simulated MTF of the optical system with f = 160 mm achromat

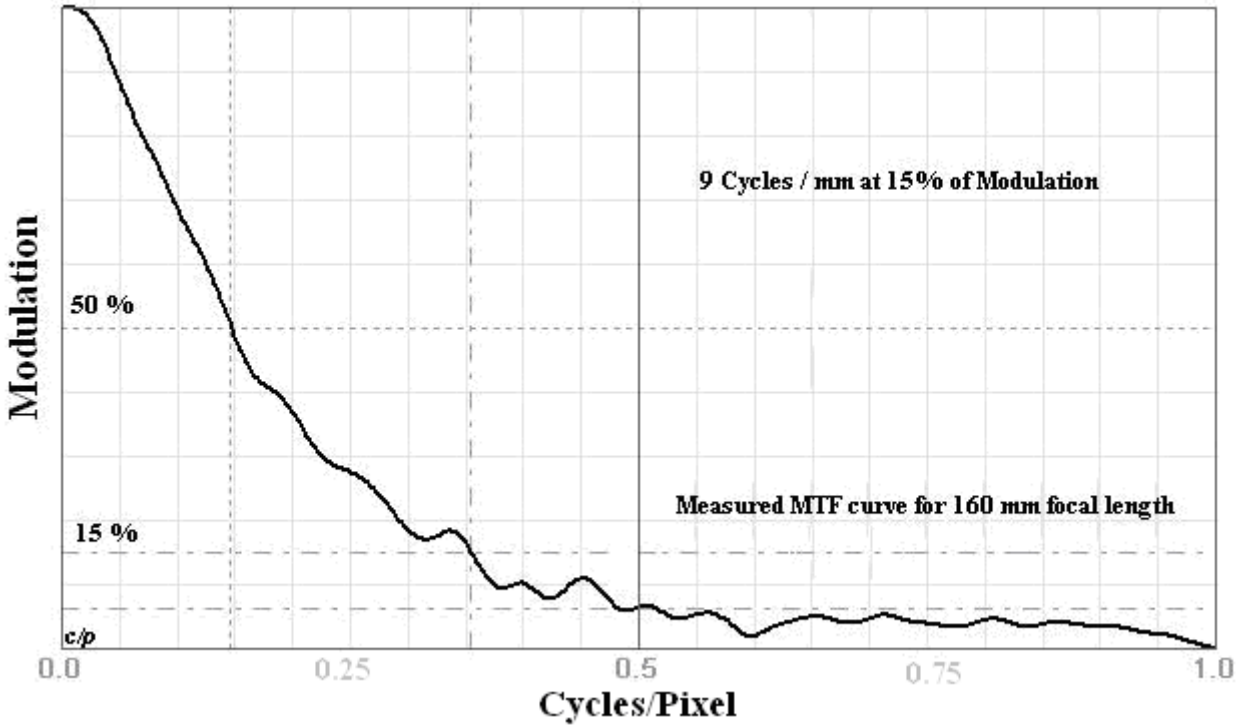

Fig19 b) Measured MTF of the optical system with f = 160 mm achromat

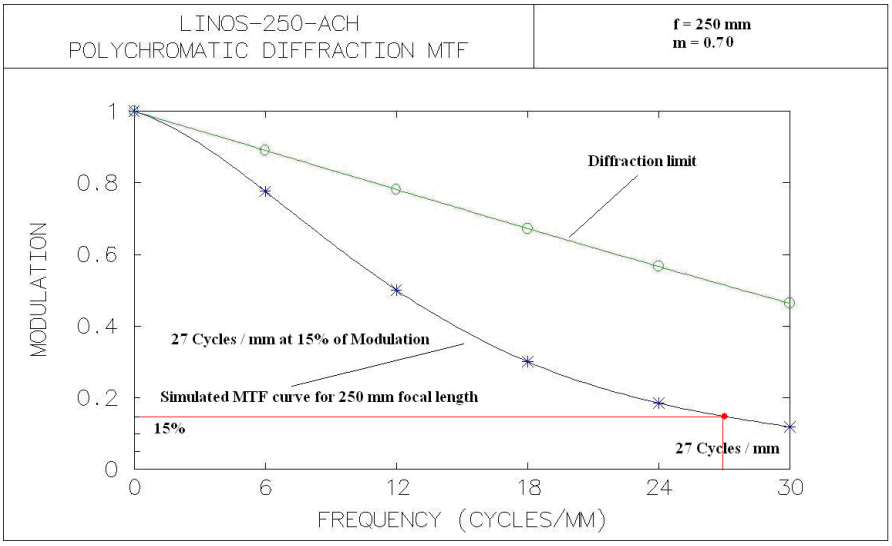

Fig19 c) Simulated MTF of the optical system with f = 250 mm achromat

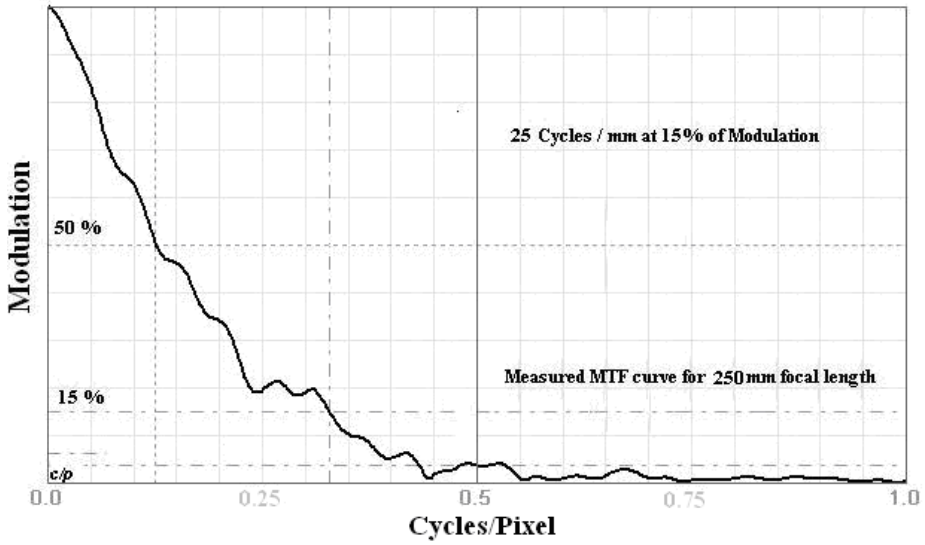

Fig19 d) Measured MTF of the optical system with f = 250 mm achromat

The measurement software calculates the MTF in cycles per pixel which was then converted by cycles/mm using the ratio between real pixel size from the plot over the projected pixel size from table2 (e.g. for f = 250 mm achromat: 0.25 cycles/pixel = 0.25/0.013 ≈ 19 cycles/pixel).One can see that there is a difference of 1cycle/mm and 2 cycles/mm between the simulated and measured values for

f=160 mm and f=250mm achromates respectively. Such difference can be originated from the errors in misalignment of the apparatus as well as the software performance. The measurement procedure was carried out in the following way:

A 1951 USAF resolution test chart [26] was placed in front of a homogeneous light source as an object; light passes through the chart and the optical line, namely achromates, and finally reaches the CCD. By moving the achromat lens across the light beam line aiming to obtain the best position for the highest resolution of the system, the CCD device was taking the images. The images were then analyzed by Quick MTF [23]. For achieving better results and finding the depth of focus of the system the lens was moved in the order of mm with steps of 0.1 mm to 0.2mm in forward and backward directions. Finally the MTF at 15% cut-off of these images were measured in cycles/mm which is considered as the resolution of the system. The setup in the lab is shown in Fig20. The simulated and measured data and for High1Scr3 are shown in table 3:

Achromat focal length	Simulated MTF at 15 % [Cycles/ mm]	Measured MTF at 15 % [Cycles / mm]
f = 160 mm	8	9
f = 250 mm	27	25

Table 3: simulation and measurement results for High1Scr3 for the PITZ beam line

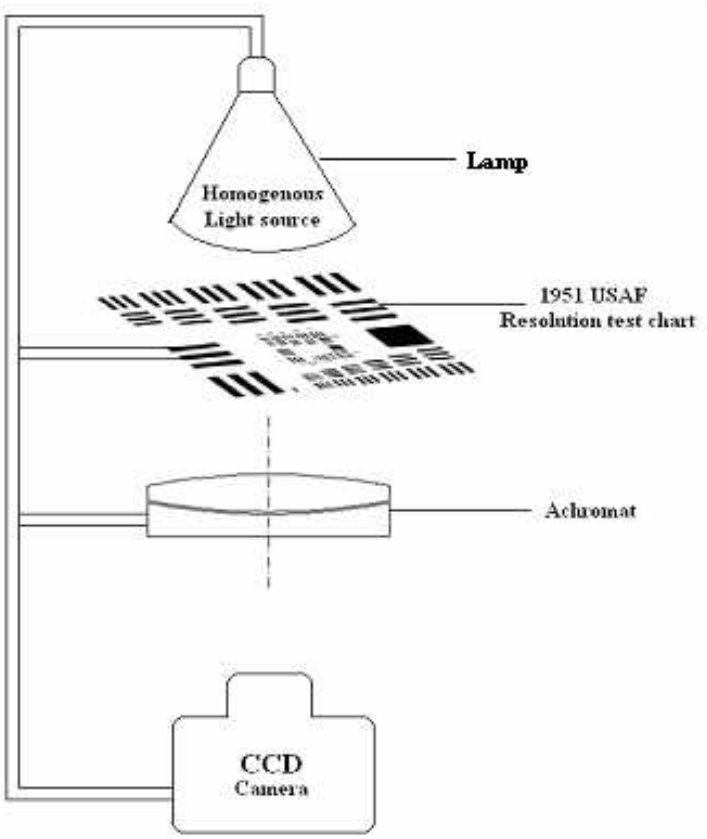

Fig20: The experimental setup in the lab

The lens displacement issue was investigated during experimental work and the following results have been achieved: One loses around 1 Cycle / 0.5 mm by extending and around 0.8 Cycle / 0.1 mm by reducing and around 0.5Cycle/0.5mm by extending and around 0.5 Cycle / 0.1 mm by reducing the fixed position of the achromates for f=160mm and f=250mm, respectively. These facts are shown in Fig21a, b.

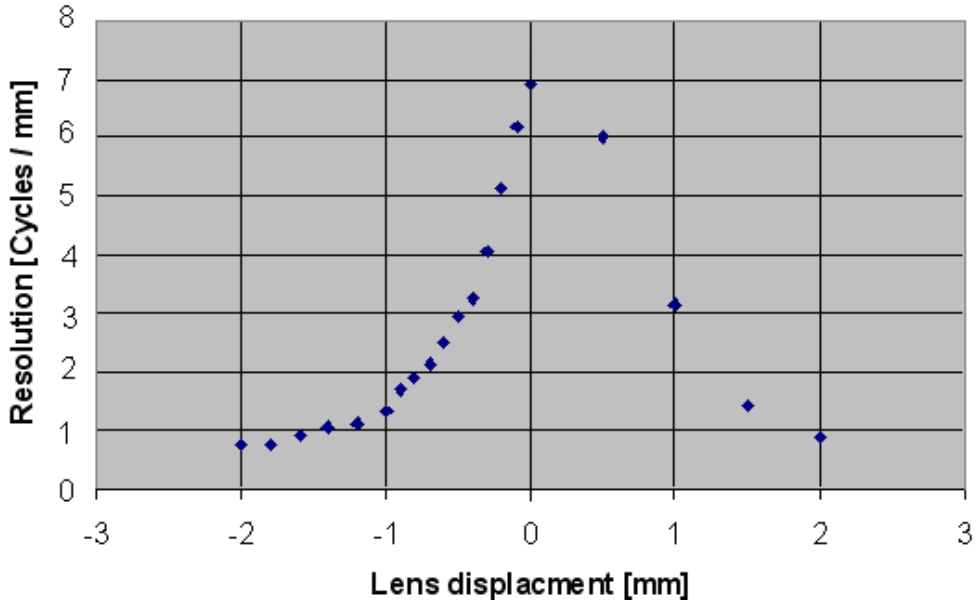

Fig21a) Lens displacement effect for f = 160 mm achromat

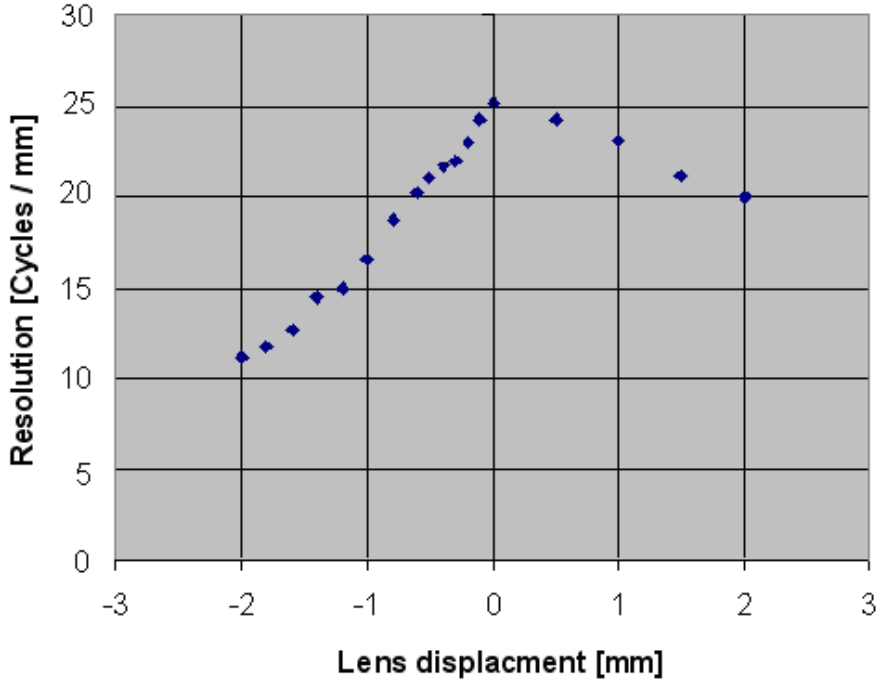

Fig21 b) Lens displacement effect for f = 250 mm achromat

From two figures above one concludes that displacement of lens plays a major role in the resolution of the system.

Another factor which affects the resolution is the diffraction and aberration limits for the lens aperture opening. For the PITZ optical system these limits were simulated and measured for differently opened aperture. The results of diffraction and chromatic aberration limits for simulated and measured values are shown in Fig22a, b, c, d.

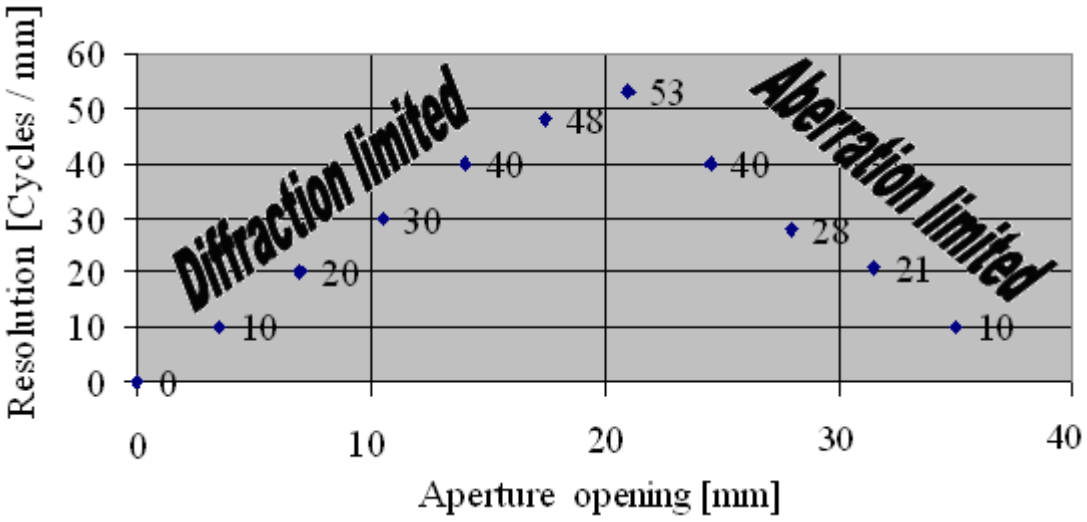

Fig22 a) Simulated diffraction and aberration limits for f = 160 mm

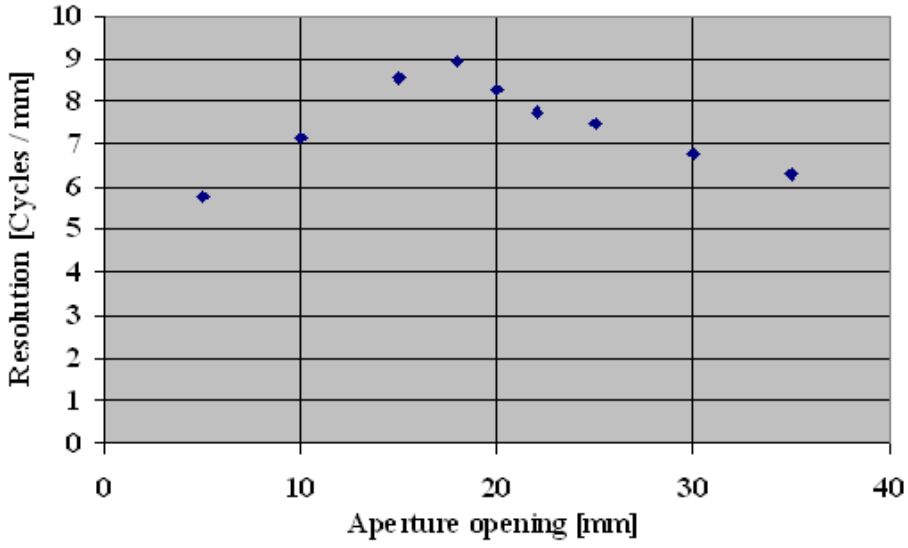

Fig22 b) Measured diffraction and aberration limits for f = 160 mm

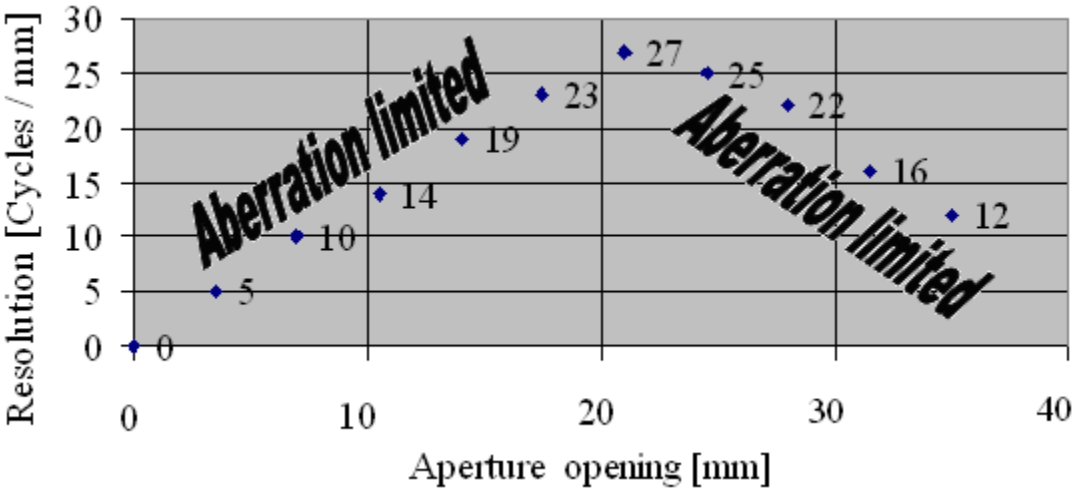

Fig22 c) Simulated diffraction and aberration limits for f = 250 mm

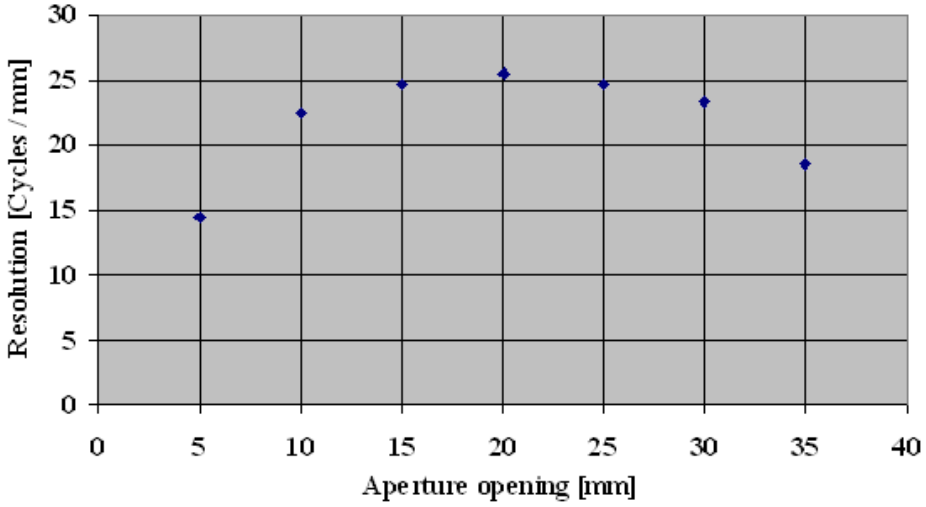

Fig22 d) Measured diffraction and aberration limits for f = 250 mm

As one can see from the Fig22a,b that there is a large absolute difference between the simulated and measured values. One can conclude that in measurement case the achromat might be placed in an out of focus area, but still one needs to study the reason in details.

Beside these measurements a recalculation of the optical line distances for the newly arrived camera namely JAI 141 for PITZ were done as well. The results shows that the full optical length needs to be decreased from 1030 mm to 910 mm (this was checked only for HighScr3) due to the higher magnification of the JAI141.In this case the achromat with f = 250mm focal length can not be used any more, because for having a real image we need at least the full optical length four times bigger than the focal length $L \geq 4f$. Instead one need to use the achromat with having f=200mm focal length. The simulation showed that 21 l/mm can be resolved by f = 200 mm achomat.

5. Conclusions

This study covers two main topics; screen performance and optical system performance. The misalignment of OTR screens towards the electron beam doesn't change the OTR distribution noticeably. The YAG photon yield depends on scattering angle which is a function of momentum and thickness of the silicon substrate which are coated by YAG powder. In YAG screens the spot size is getting larger while going to higher thicknesses which results in image blurring. Better resolution from YAG requires low scattering angle ←→ thinner layers and the silicon substrates.

The resolution of the optical system depends on the magnification power of the achromats. To achieve better resolution one should use achromates with higher magnification, but this leads to a loss in the light intensity per pixel of the camera. The achromat with 160 mm focal length resolves 9 l/mm and 8 l/mm for measurement and simulation respectively, were the achromat with 250 mm focal length resolve 25 l/mm and 27 l/mm for measurement and simulation respectively.

Lens displacement plays the major role in the resolution of the image. One loses around 1 Cycle / 0.5 mm by extending and around 0.5 Cycle / 0.1 mm by reducing, around 0.5 Cycle / 0.5 mm by extending and around 1 Cycle / mm by reducing the fixed position of the achromates for f = 160 mm and f = 250 mm,

respectively. The aperture opening might be consider as a technique for achieving better resolution, but one is limited in opening and closing it to some extent because of diffraction and aberration limits. For the PITZ case 21mm is the optimum opening aperture for both achromates which showed the highest resolution value in the measurements for a screen with 90° to the screen axis. This optimum may defer in the case of a 45° screen because of having a depths of focus problem.

Further studies are required to find the resolution of the system by taking images directly from the camera during camera running and connect the MTF cut-off of the system to the resolution. One needs to study how to map the screen on the CCD by using some MATLAB or GEANT4 codes.

Bibliography

1. S.Roman, Transverse beam size measurement systems at Photo Injector Test Facility in Zeuthen, Master thesis, Zeuthen, 2007, Germany.
2. World particle accelerators, http://elsa.physik.uni-bonn.de/
3. J.W.Bähr, et al. Recent upgrade of the PITZ facility, Zeuthen, 2010, Germany.
4. European XFEL project, http://xfel.eu.de/
5. J.Buon, Beam phase space and emittance, CERN Accelerator School, Finland, 1992.
6. Understanding MTF, http://normankoren.com/Tutorials/MTF.html
7. Depth of focus and depth of field, http://inst.eecs.berkeley.edu/
8. Lens diffraction and photography, http://cambridgeincolour.com/tutorials/ diffraction-photography.htm
9. Abberrations, http://hyperphysics.phy-astr.gsu.edu/hbase/geoopt/ aberrcon.html/
10. Aberrations, http://microscopyu.com/tutorials/java/aberrations/chromatic/
11. Chromatic Aberrations, http://en.academic.ru/dic.nsf/enwiki/34883/
12. Machine beam line design, http://pitz.desy.de/
13. G.Beth, Optical Transition Radiation, UCLA Department of physics, Los Angles, CA 9002, USA.
14. K.Honkavaara, PhD thesis, LAL Orsay, 1995, France.

15. M.Hibino, K.Irie, R.Autrata, and P.Schauer, Characteristics of YAG Single Crystals for Electron Scintillators of STEM, Department of Electronics. School of Engineering. Nagoya University. Furo-cho. Chikusa-ku, Nagoya, 464-01, Japan.
16. A.Murokh, J.Rosenzweig, Limitations on the resolution of YAG:Ce beam profile monitor for high brightness electron beam.
17. Beer's law, http://teaching.shu.ac.uk/hwb/chemistry/tutorials/molspec/beers1.htm/
18. Aperture, Wiki Photos.
19. K.Sirgiy et al., Design and construction of the multipurpose dispersive section at PITZ, DESY Zeuthen, 2006, Germany.
20. Data and figures given by the mechanics group of PITZ, Zeuthen, 2010, Germany.
21. C.Amsler et al., Particle physics booklet, Particle Data Group, Physics Letters B667, 2008.
22. OSLO EDU Software, http://lambdares.com/
23. Quick MTF, Lens testing software, http://quickmtf.com
24. Achromat, http://linos.de
25. Prosilica 1350, http://prosilica.com/

26. USAF-1951 Test-Chart, http:// scandig.de/zubehoer/targets/usaf-1951-test-chart-scanner-aufloesung.html

Acknowledgments

First and foremost I offer my sincerest and gratitude to my supervisors, Prof.Dr.Claus Grupen and Dr.Frank Stephan, who have supported me throughout my thesis, with their patience and knowledge. With out their encouragement and effort this thesis would not have been completed or written.

I am grateful of Yevgeniy Ivanisenko and Galina Assova who had extremely helped me carrying out this work. They both put too much effort together in order to encourage me treating different problems in simple ways. I thank Dr.Juergen.Bahr, Dr.Mikhail Krasilnikov, Dr.Hans – Juergen Grabosch, Dr.Sakhron Rimjaem, Dr.Marc Hanel, Grygorii Vashchenko, Dr.Martin Khojoyan, Dr.Marek Otevrel and all PITZ group members from scientific persons to engineers and technicians who have helped me and provided me with useful and demanded information in time.

My special thanks are regarded to my great teachers and life guides Prof.Dr.H.D.Dahmen who simply enabled me to study in German academic environment and Prof.Msc.Zalmai Ahmadzai who encouraged and guided me throughout my whole scientific life. I am sure without their guidance; I won't be able to have a University level education.

Finally, I wish to thank my great parents and my whole respectful family for their warm support during my studies period. I attribute my master degree to my late mother and father who warmly supported me financially and gave a lot of love and encouragement to keep studying in any hard situations.